

[¹¹C]-(R)PK11195 tracer kinetics in the brain of glioma patients and a comparison of two referencing approaches

Zhangjie Su · Karl Herholz · Alexander Gerhard ·
Federico Roncaroli · Daniel Du Plessis · Alan Jackson ·
Federico Turkheimer · Rainer Hinz

Received: 18 March 2013 / Accepted: 30 April 2013 / Published online: 29 May 2013
© The Author(s) 2013. This article is published with open access at Springerlink.com

Abstract

Purpose Translocator protein (TSPO) is a biomarker of neuroinflammation that can be imaged by PET using [¹¹C]-(R)PK11195. We sought to characterize the [¹¹C]-(R)PK11195 kinetics in gliomas of different histotypes and grades, and to compare two reference tissue input functions (supervised cluster analysis versus cerebellar grey matter) for the estimation of [¹¹C]-(R)PK11195 binding in gliomas and surrounding brain structures.

Methods Twenty-three glioma patients and ten age-matched controls underwent structural MRI and dynamic [¹¹C]-(R)PK11195 PET scans. Tissue time–activity curves (TACs) were extracted from tumour regions as well as grey matter (GM) and white matter (WM) of the brains. Parametric maps of binding potential (BP_{ND}) were generated with the simplified reference tissue model using the two input functions, and were compared with each other. TSPO expression was assessed in tumour tissue sections by immunohistochemistry.

Results Three types of regional kinetics were observed in individual tumour TACs: GM-like kinetics ($n=6$, clearance of the tracer similar to that in cerebellar GM), WM-like kinetics ($n=8$, clearance of the tracer similar to that in cerebral WM) and a form of mixed kinetics ($n=9$, intermediate rate of clearance). Such kinetic patterns differed between low-grade astrocytomas (WM-like kinetics) and oligodendrogliomas (GM-like and mixed kinetics), but were independent of tumour grade. There was good agreement between parametric maps of BP_{ND} derived from the two input functions in all controls and 10 of 23 glioma patients. In 13 of the 23 patients, BP_{ND} values derived from the supervised cluster input were systematically smaller than those using the cerebellar input. Immunohistochemistry confirmed that TSPO expression increased with tumour grade.

Conclusion The three types of [¹¹C]-(R)PK11195 kinetics in gliomas are determined in part by tracer delivery, and indicated that kinetic analysis is a valuable tool in the study of gliomas with the potential for in vivo discrimination between low-grade astrocytomas and oligodendrogliomas. Supervised cluster and cerebellar input functions produced consistent BP_{ND} estimates in approximately half of the gliomas investigated, but had a systematic difference in the remainder. The cerebellar input is preferred based on theoretical and practical considerations.

Z. Su (✉) · K. Herholz · A. Gerhard · A. Jackson · R. Hinz
Wolfson Molecular Imaging Centre, University of Manchester,
27 Palatine Road,
Manchester, UK
e-mail: zhangjie.su@manchester.ac.uk

F. Roncaroli
“John Fulcher” Neuro-Oncology Lab, Imperial College London,
Charing Cross Campus, St Dunstons Road,
London, UK

D. Du Plessis
Neuropathology Unit, Salford Royal NHS Foundation Trust,
Stott Lane,
Salford, UK

F. Turkheimer
Centre for Neuroimaging, Institute of Psychiatry,
King’s College London, De Crespigny Park,
London, UK

Keywords Translocator protein · [¹¹C]-(R)PK11195 ·
Kinetic analysis · Reference tissue · Glioma · PET

Introduction

Translocator protein (TSPO), formerly known as peripheral benzodiazepine receptor, is an 18-kDa mitochondrial membrane protein mainly expressed in cells of the mononuclear phagocyte lineage [1, 2]. In the normal central nervous

system, TSPO expression is low and limited to vessels, perivascular macrophages and ependyma [3, 4]. In contrast, its expression increases considerably in microglia/macrophages in pathological conditions when any insult to brain tissue has occurred [5]. For this reason, TSPO is regarded as a reliable biomarker of neuroinflammation for the detection of active pathological processes [1].

[¹¹C]-(R)PK11195 is a highly selective radioligand for TSPO [6] and has been used extensively with PET for in vivo visualization of microglial activation in acute and chronic inflammatory as well as noninflammatory brain disorders [3, 7–13]. [¹¹C]-(R)PK11195-specific binding is minimal in normal brain but increases significantly in areas of neuroinflammation. Different methods of kinetic modelling for quantification of [¹¹C]-(R)PK11195 binding have been assessed. Kropholler et al. [14, 15] recommended a reversible two-tissue compartment model with K_1/k_2 fixed to the whole cortex when a metabolite-corrected arterial plasma input function is available, whilst the simplified reference tissue model (SRTM [16]) is considered the best alternative in the absence of an arterial input function. Schuitemaker et al. [17] found that the basis function implementation of SRTM [18] performed the best amongst reference tissue techniques for generating parametric images of [¹¹C]-(R)PK11195 binding potential. Given the expression of TSPO in endothelial cells and smooth muscle, a modified SRTM with blood volume term was subsequently developed to account for differences in vascular binding, not only between reference and target regions but also amongst study cohorts [19].

The SRTM does not require a plasma input function, and therefore there is no need for arterial cannulation. It aims to provide a measure of specific binding. However, the model relies on the assumptions that: (1) a reference region devoid of specific binding exists, and (2) the nonspecific binding is the same in both the reference and target regions. Some studies have adopted the cerebellum as a standard reference tissue [2, 10, 20–22], although it has been argued that the cerebellum may be inappropriate due to the possible presence of activated microglia in certain brain disorders [15, 23], and the presence of TSPO in vessels which cannot be resolved with the spatial resolution of clinical PET scanners. Cluster analysis, a ‘data-driven’ approach, was introduced as an alternative for the extraction of normal tracer kinetics to serve as a reference region input function and was adopted for [¹¹C]-(R)PK11195 studies [7, 24, 25] in the form of unsupervised cluster analysis. In order to extract as reference tissue a cluster of grey matter voxels devoid of both specific binding and spurious signals (particularly from the blood pool and muscle), Turkheimer et al. [4] then developed a supervised clustering approach using six predefined kinetic classes, that is for normal grey matter (GM), white matter (WM), skull, muscle, blood pool and pathological TSPO binding. This technique combined with SRTM has been shown to produce highly reproducible and

reliable estimates of [¹¹C]-(R)PK11195 binding in healthy volunteers and patients with Huntington’s disease [4]. Furthermore, a modified supervised cluster algorithm has been proposed, focusing on brain tissue with only four kinetic classes (previous skull and muscle classes omitted) to improve its performance [26]. Nonetheless, developments in kinetic methodology are still ongoing with the aim of validating the appropriate plasma and reference region compartmental models for organs and pathologies that have not yet been studied.

TSPO expression has also been investigated in gliomas. Pathological studies on surgical samples of astrocytoma have demonstrated that TSPO is expressed predominantly in neoplastic cells and it is higher in WHO grade III and IV lesions [27, 28]. In contrast, there are no published data on TSPO expression in oligodendrogliomas. Only three PET studies using [¹¹C]-PK11195 have so far been performed [29–31] in a small number of patients with astrocytoma. These studies have shown conflicting results, suggesting either increased or decreased [¹¹C]-PK11195 uptake in the tumours. Different kinetic modelling approaches in these studies might have accounted for the inconsistent findings, and detailed characterization of tracer behaviour within the tumours is not available, particularly for low-grade gliomas (LGG).

In the present study, we therefore examined patients with LGG or high-grade gliomas (HGG) of different subtypes (mainly astrocytoma and oligodendroglioma) to investigate systematically [¹¹C]-(R)PK11195 kinetics in the tumours, using the SRTM comparing supervised clustered GM and cerebellar GM as reference tissue input functions. Our hypothesis was that different histotypes and grades of gliomas could be discriminated by differences in [¹¹C]-(R)PK11195 kinetics. Such discrimination is still a challenge with conventional contrast CT and MR imaging in clinical practice. Therefore, we investigated whether [¹¹C]-(R)PK11195 tracer kinetic analysis can provide this information, and which reference tissue input function is more suitable for glioma studies.

Materials and methods

Patients and control subjects

The study group recruited comprised 23 patients (mean age 40 years, age range 22 – 73 years; 16 men, 7 women) with histologically proven glioma (clinical information is provided in Tables 1 and 2). None of the patients had concurrent systemic disease, and none of them had had surgical intervention, radiotherapy or chemotherapy prior to PET scanning. None of the patients were taking benzodiazepines. Nine patients were taking dexamethasone. In seven of these patients it was stopped for at least 2 weeks prior to the PET scan because of its potential suppressive effect on microglial

Table 1 Clinical characteristics, [¹¹C]-(R)PK11195 kinetics and immunoperoxidase results in 14 patients with LGG

Patient ID	Age (years)	Sex	Histology	WHO grade	Tumour location	Gadolinium enhancement	Tumour TAC	TSPO(+) tumour cells	Iba1(+) microglia
1	41	M	O	II	Frontal-temporal lobe (right)	No	Mixed	++	++
2	25	F	A	II	Frontal lobe (right)	No	WM-like	++	++
4	45	M	O	II	Medial temporal lobe (right)	No	Mixed	Not enough tissue	
5	24	F	OA	II	Parietal lobe (right)	No	WM-like	++	++
6	40	M	O	II	Frontal lobe (right)	No	GM-like	+	++
7	73	F	Not operated	LGG	Thalamus (left)	No	Mixed	No tissue	
8	63	F	A	II	Parietal, frontal, temporal lobe (left)	No	GM-like	++	++
9	33	M	A	II	Posterior frontal lobe (right)	No	WM-like	++	++
11	30	M	O	II	Posterior frontal lobe (right)	No	Mixed	++	++
12	47	F	A	II	Temporal lobe (left)	No	WM-like	++	++
17	33	M	A	II	Frontal lobe (left)	No	WM-like	++	++
18	42	M	OA	II	Temporal lobe (left)	No	Mixed	++	++
20	24	M	O	II	Frontal-temporal lobe (right)	No	Mixed	+	++
22	50	F	O	II	Frontal lobe (left)	No	GM-like	++	+++

A astrocytoma, O oligodendroglioma, OA oligoastrocytoma

activation [32–34], but in two (patients 16 and 20) discontinuation was considered clinically contraindicated. Ten healthy volunteers (mean age 44 years, age range 23 – 68 years; 7 men, 3 women) were also scanned. Their past medical history was unremarkable; they all had normal physical and neurological examinations and showed no significant structural lesions on anatomical MRI as judged by an experienced neuroradiologist (A.J.).

Written informed consent was obtained from all participants. This study was approved by the Wrightington, Wigan and Leigh Ethics Committee as well as the University of Manchester Ethics Committee. Permission to administer radioisotopes was granted by the Administration of Radioactive Substances Advisory Committee of the Department of Health (ARSAC), UK.

Volumetric MRI

All subjects underwent a structural MRI scan within 1 month before the PET procedure. High-resolution 3-D T1-weighted spoiled gradient recalled echo and inversion recovery (IR) sequences were acquired on a 3-T (patients) or a 1.5-T (controls) scanner (Philips Achieva; Philips Medical Systems, Best, The Netherlands). The protocol for patients also included standard anatomical imaging, i.e. T2-weighted and fluid-attenuated inversion recovery (FLAIR) sequences, and gadolinium (Gd) contrast-enhanced images.

[¹¹C]-(R)PK11195 production and PET acquisition

[¹¹C]-(R)PK11195 (1-(2-chlorophenyl)-N-methyl-N-(1-methylpropyl)-3-isoquinoline carboxamide) was synthesized

Table 2 Clinical characteristics, [¹¹C]-(R)PK11195 kinetics and immunoperoxidase results in nine patients with HGG

Patient ID	Age (years)	Sex	Histology	WHO grade	Tumour location	Gadolinium enhancement	Tumour TAC	TSPO(+) tumour cells	Iba1(+) microglia
3	37	M	AA	III	Frontal-temporal lobe (right)	None	WM-like	++	++
10	42	M	AA	III	Posterior frontal lobe (left)	Focal	Mixed	++	++
13	46	M	AA	III	Parietal lobe (left)	Focal	Mixed	++	++
14	57	M	GBM	IV	Posterior frontal lobe (left)	Focal	Mixed	+++	+++
15	22	M	A OA	III	Frontal-parietal lobe (right)	Minor	GM-like	++	++
16	41	M	GBM	IV	Temporal-occipital lobe (right)	Massive	WM-like (high)	+++	+++
19	52	M	AA	III	Parietal lobe (left)	Minor	GM-like	+++	+++
21	40	F	GBM	IV	Frontal lobe (right)	Massive	WM-like (high)	+++	+++
23	24	M	AO	III	Frontal-temporal lobe (left)	Minor	GM-like	++	++

AA anaplastic astrocytoma, AO anaplastic oligodendroglioma, A OA anaplastic oligoastrocytoma, GBM glioblastoma

as described previously [6, 35]. All PET scans were performed on a high-resolution research tomograph (HRRT; Siemens/CTI, Knoxville, TN). The axial and transaxial fields of view of this 3-D dedicated brain scanner were 25 cm and 35 cm, respectively, giving an intrinsic spatial resolution of approximately 2.5 mm. A 7-min transmission scan using a ^{137}Cs point source was acquired for subsequent attenuation and scatter correction. Shortly after the start of the emission scan, [^{11}C]-(*R*)PK11195 was injected intravenously as a slow bolus over approximately 15 s. The administration parameters in patients and controls are given in Table 3. Emission data were then acquired over 60 min in list mode as 18 time-frames (one background frame of approximately 7 min prior to injection, followed by 17 frames: 1×15 s, 1×5 s, 1×10 s, 1×30 s, 4×60 s, 7×300 s and 2×600 s). The subject's head position was indicated (using laser beams) and monitored (via a camera) throughout the scan and corrected immediately if necessary.

Image reconstruction and analysis

The multiframe PET images were reconstructed with the iterative ordinary Poisson ordered-subset expectation maximization (OP OSEM) 3-D algorithm, incorporating normalization and corrections for random coincidences, scattered radiation and attenuation [36]. For reconstruction 16 subsets were used, and the reconstruction was run for 12 iterations for the mean activity concentration value at the volume-of-interest level to converge. The voxel size of the reconstructed PET images was $1.22 \times 1.22 \times 1.22$ mm³. After reconstruction, images were regularized with a 3-D gaussian filter of 4 mm full-width at half-maximum to reduce image noise at the voxel level prior to calculation of parametric maps with the SRTM [37].

Individual MRI scans were coregistered with the summed PET images [38], and the T1-weighted IR images were segmented into GM and WM probability maps [39]. The inverse transformation parameters from segmentation were used to warp a maximum probability brain atlas [40, 41] into individual space. The quality of the coregistration, segmentation and normalization was visually inspected for accurate anatomical colocalization. On observation, the warped brain atlas was

distorted regionally in the tumours and their margin as expected, but matched the extratumoral structures well, especially in the cerebral hemisphere contralateral to the tumour and in the cerebellum. Any mismatch in extratumoral structures was corrected manually. Then the GM probability map was binarized using a 0.5 threshold and applied as a mask to the brain atlas, from which an individualized GM atlas was created. Both atlases were used to sample the ratio of influx (R_i , representing the ratio of tracer delivery to the target region to delivery to the reference region) and binding potential (BP_{ND} , representing the ratio of specifically bound radioligands to nondisplaceable ones in tissue at equilibrium [16, 42]) values from parametric images. Given the unpredictable spatial distribution of activated microglia in disease, the pixel-by-pixel generation of parametric images was preferred over the calculation of binding parameters from time-activity curves (TACs) extracted from anatomical regions of interest (ROIs) in our study [43].

For practical reasons, no arterial input function was obtained (unavailability of reliable analysis for radiolabelled metabolites of [^{11}C]-(*R*)PK11195 at the time of study setup, and potential reduction in recruitment of patients with HGG whose time window for participation prior to surgical interventions was short). Two different reference input functions were used: (1) a cluster of GM voxels extracted from the supervised clustering algorithm [4], and (2) total GM of the bilateral cerebellum, as it is a large and relatively homogeneous structure distant from the tumours [44, 45]. The BP_{ND} parametric images obtained using different reference tissue input functions were compared with each other.

Each tumour (including visible oedema, if present) was manually delineated on the coregistered T2-weighted FLAIR MR image and confirmed against the T1-weighted contrast-enhanced MR image. A region of WM was also drawn in the contralateral centrum semiovale. These ROIs, together with the individualized GM atlas, were projected onto parametric images and dynamic PET volumes to extract group mean R_i and BP_{ND} values as well as TACs from the tumours, centrum semiovale WM and cerebellar GM. Individual tumour TACs were compared with corresponding GM and WM TACs, from which radioactivity ratios of tumour to GM (tumour/GM) and tumour to WM (tumour/WM) were obtained for each temporal frame. Then the time-courses of tumour/GM and tumour/WM ratios from radioactivity peak to scan end were outlined for each scan, and mean tumour/GM and tumour/WM ratios were calculated by weighting the ratios against the frame lengths. Group means (average of the mean ratios of all scans) and standard deviations (SD) were also derived.

Pathological assessments

The extent of TSPO expression and microglial/macrophagic infiltrate was characterized semiquantitatively on the tissue sections of 21 tumours using immunoperoxidase

Table 3 Age and [^{11}C]-(*R*)PK11195 administration parameters (means \pm SD; no significant differences between glioma patients and healthy volunteers)

Variable	Glioma patients ($n=23$)	Healthy volunteers ($n=10$)
Age (years)	40 \pm 13	44 \pm 15
Injected dose (MBq)	517 \pm 127	549 \pm 124
Specific activity (GBq/ μmol)	130 \pm 48	111 \pm 56
Injected mass of stable PK11195 (μg)	1.6 \pm 0.8	2.4 \pm 2.1
Radiochemical purity (%)	98.4 \pm 0.9	98.3 \pm 0.9

immunohistochemistry with antibodies against TSPO (goat polyclonal, GeneTex; dilution 1:750) and Iba1 (rabbit polyclonal, WAKO/019-19741; dilution 1:500), respectively. In patient 4, the tissue left after routine neuropathological assessments was too small for immunostaining.

TSPO-positive and TSPO-negative neoplastic cells were identified by their nuclear morphology (hyperchromatic nucleus). We assigned a score of 3+ to lesions showing more than 25 % TSPO-positive tumour cells, a score of 2+ to those showing expression between 5 and 25 % and a score 1+ to those showing only scattered positive cells (less than 5 %). Perivascular macrophages and endothelial cells in the tissue adjacent to the tumour were considered as positive control. Neoplastic cells showed different staining intensities, but this parameter was difficult to assess semiquantitatively. Haemorrhagic areas, microcysts and necrosis as well as the fields at the edge of tissue sections were avoided.

A similar method was used to assess the number of microglia identified with the immunostaining for Iba1, a calcium-dependent molecule that is a widely recognized marker of macrophages and microglia and is known to be expressed in ramified, quiescent to fully activated microglia [46]. Only a few microglia expressed TSPO but an accurate estimate of TSPO-positive microglia could not be achieved using immunoperoxidase immunohistochemistry.

Statistical analysis

All data are expressed as means \pm SD. [^{11}C]-(*R*)-PK11195 uptake parameters in different kinetics were compared using the Kruskal-Wallis test with post hoc tests. BP_{ND} parametric images generated using different input functions were compared pixel-by-pixel using Bland-Altman plots [47] with local regression [48]. Regional BP_{ND} values derived from the two input functions were compared using a general linear model (GLM, repeated measures) with input function and region as within-subjects variables. A probability value of $p < 0.05$ was considered statistically significant.

Results

Tracer kinetic analysis

Injection of [^{11}C]-(*R*)-PK11195 resulted in a rapid initial peak of activity in the TACs. After this peak, the TACs of cerebellar GM (Fig. 1a, red lines) exhibited a sharp decline in radioactivity over the first 3 min, followed by a gradual decrease to the end of scanning, falling to, or below, the level of the WM TACs during the last 25 min. Similar initial peaks (reaching 45 – 73 % of the level of cerebellar GM) and fast washout in the next 3 – 5 min were also seen in the TACs of the contralateral centrum semiovale WM (Fig. 1a,

amber lines). Subsequently the amount of radioactivity reached a plateau and stayed at this low background level throughout the scan, indicating slow clearance of the tracer. The TACs of normal GM and WM in patients appeared similar to those in healthy volunteers.

In gliomas, the initial tracer uptake peaked at least to the level of that in WM in all patients, despite variable amounts of radioactivity in the tumour regions across subjects. Three types of regional kinetics were found in individual tumour TACs (Fig. 1): GM-like kinetics ($n=6$, tracer clearance similar to that in the cerebellar GM; group mean tumour/GM ratios 1.12 ± 0.08 and tumour/WM ratios 1.39 ± 0.14), WM-like kinetics ($n=8$, tracer clearance similar to that in the WM, with a slight descent after the plateau at the midway time points, i.e. 30 – 40 min; group mean tumour/GM ratios 0.81 ± 0.29 and tumour/WM ratios 0.97 ± 0.31), and mixed kinetics ($n=9$, intermediate rate of clearance; group mean tumour/GM ratios 0.92 ± 0.11 and tumour/WM ratios 1.10 ± 0.16). In addition to the typical examples illustrated in Fig. 1, variable levels of [^{11}C]-(*R*)-PK11195 uptake within the tumours led to a few atypical TAC shapes in the WM-like kinetic type, where two glioblastomas (GBMs) with massive Gd enhancement in the contrast MR images displayed WM-like kinetics at a level approximately 0.5-fold higher than the WM throughout the acquisition (Fig. 2). Kinetic classification of such cases relied more on visual inspection of the TACs rather than on calculation of mean tumour/GM and tumour/WM ratios. In general, the three types of tracer kinetics were independent of glioma grades, but appeared to differ between different histological subtypes in tumours without Gd enhancement on MRI indicating an intact blood–brain barrier (BBB). Four of five low-grade astrocytomas displayed WM-like tracer kinetics within the tumours, whilst the six low-grade oligodendrogliomas demonstrated mixed or GM-like kinetics (Tables 1 and 2).

R_1 values of whole tumour ROIs were calculated using either cerebellar GM or the supervised cluster of GM as reference tissue (expressed as $R_1^{\text{cerebellum}}$ and R_1^{super} , respectively). $R_1^{\text{cerebellum}}$ and R_1^{super} were separated evenly into three categories (high, moderate and low) based on the range of values and linked to the three types of tumour kinetics (Fig. 3). With the cerebellar input function, all four tumours (100 %) with high $R_1^{\text{cerebellum}}$ showed GM-like TACs. six of seven tumours (86 %) with low $R_1^{\text{cerebellum}}$ showed WM-like TACs and the remaining one showed a mixed TAC. Of 12 tumours with moderate $R_1^{\text{cerebellum}}$, eight (67 %) showed mixed TACs, whereas two showed GM-like TACs and two showed WM-like TACs. With the supervised cluster input function, five of seven tumours (71 %) with high R_1^{super} showed GM-like TACs and the remaining two showed mixed TACs. All four tumours (100 %) with low R_1^{super} showed WM-like TACs. Of 12 tumours with moderate R_1^{super} , seven (58 %) showed mixed TACs, whereas one showed a GM-like TAC

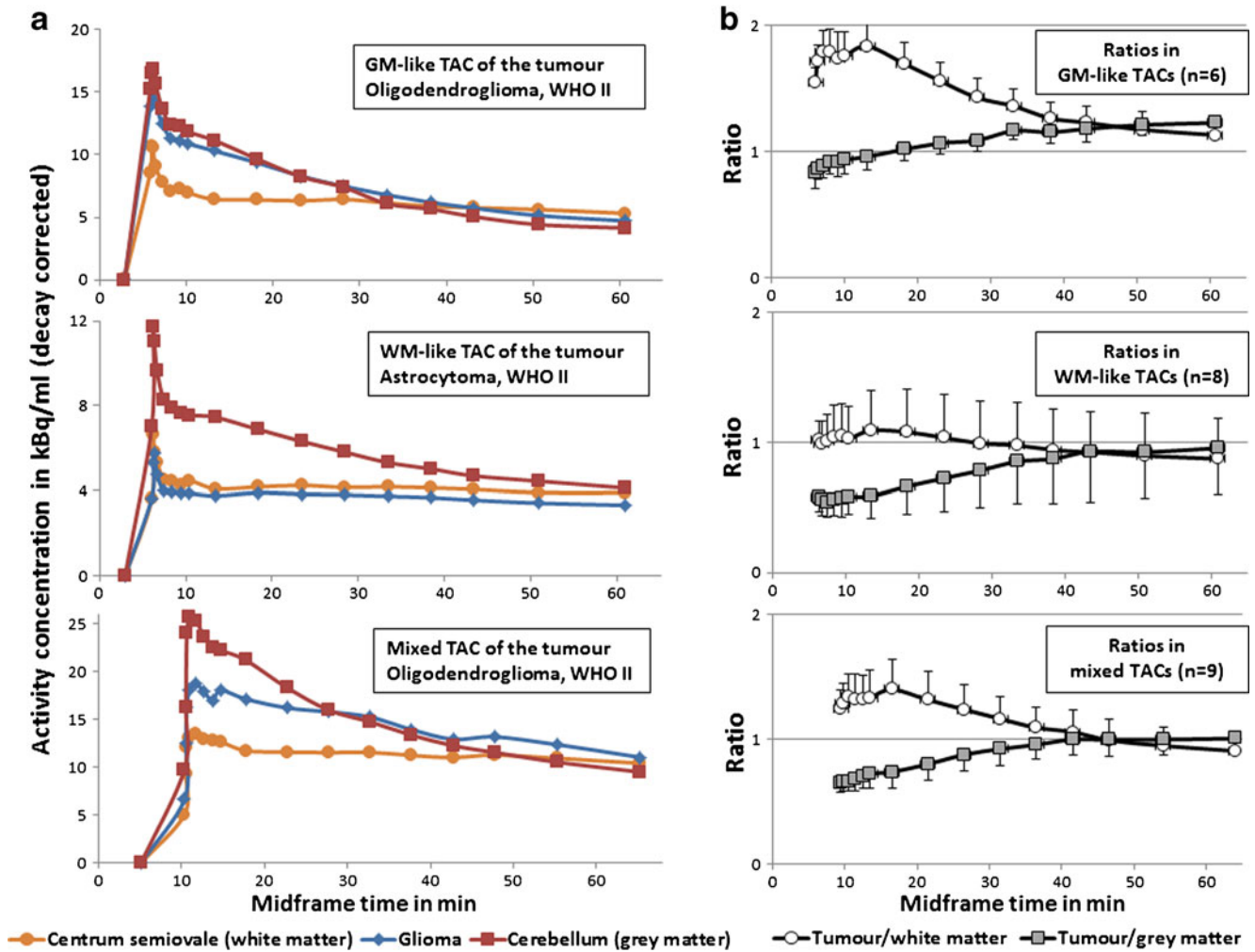


Fig. 1 **a** Representative tumour TACs of the three kinetic types from three example scans. Radioactivity concentration was plotted against frame midpoints. **b** Time-course (from the initial peak to scan end) of

the tumour/GM (cerebellum) and the tumour/WM (centrum semiovale) ratios of the three kinetic types, plotted as means ± SD

and four showed WM-like TACs. The Kruskal-Wallis test showed a significant effect of TAC grouping on both $R_1^{cerebellum}$ and R_1^{super} estimates ($p=0.003$ and 0.001 , respectively), where the mean $R_1^{cerebellum}$ or R_1^{super} of each TAC type differed (all $p<0.05$).

Albeit closely correlated ($r=0.95$, $p<0.0001$), tumour R_1^{super} was generally lower than tumour $R_1^{cerebellum}$, indicating certain differences in the two reference regions. The influence of different reference regions on BP_{ND} estimates was investigated as discussed in the following sections.

Supervised cluster analysis versus cerebellum as reference

Healthy volunteers

Pixel-by-pixel comparisons of BP_{ND} parametric maps derived from supervised cluster analysis (BP_{ND}^{super}) and cerebellar GM ($BP_{ND}^{cerebellum}$) as input function are shown in

Fig. 4. In Bland-Altman plots the majority of the points clustered closely around zero, with a generally horizontal line of local regression in each case (Fig. 4b). This finding is in keeping with the observation that TACs of the two reference regions mostly overlap (Fig. 4c), thus resulting in similar BP_{ND} estimates, despite the difference during the first 20 min. The first peak in both TACs reflected the initial peak from the vascular signals, while the second peak in the TACs of the supervised cluster represented tracer reperfusion and uptake in the tissue (Fig. 4c). BP_{ND}^{super} and $BP_{ND}^{cerebellum}$ values were sampled from 12 ROIs (temporal lobe, frontal lobe, occipital lobe, parietal lobe, thalamus and putamen in the left and right hemispheres). GLM analysis revealed neither an effect of input function on BP_{ND} ($F=0.027$, $p=0.874$) nor any cross effects between the input function and region or side, indicating that BP_{ND}^{super} did not differ from $BP_{ND}^{cerebellum}$ across all ROIs in the control subjects.

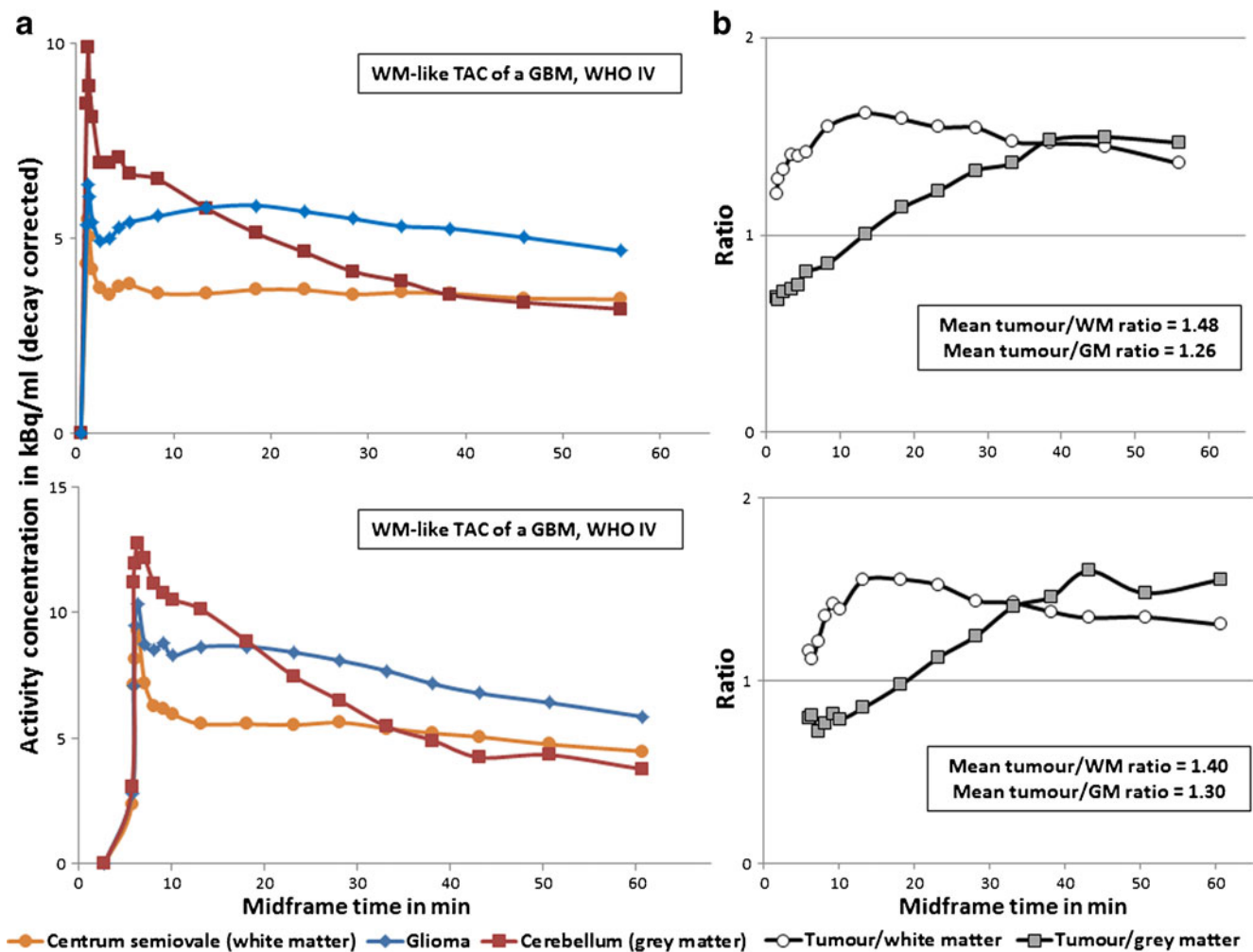


Fig. 2 **a** Tumour TACs of two GBMs (with massive Gd enhancement in the contrast MRI) that displayed WM-like kinetics at a high level of radioactivity concentration (approximately 0.5-fold higher than that in

WM), plotted against frame midpoints. **b** Corresponding time-course (from the initial peak to scan end) of tumour/GM (cerebellum) and tumour/WM (centrum semiovale) ratios in the two patients

Glioma patients

BP_{ND}^{super} and $BP_{ND}^{cerebellum}$ values were sampled from eight ROIs (tumour, ipsilateral cerebral hemisphere excluding the tumour region, and temporal lobe, frontal lobe, occipital lobe, parietal lobe, thalamus and putamen in the contralateral hemisphere). GLM analysis showed a significant effect of input function on BP_{ND} estimates ($F=16.94$, $p=0.0005$) and a cross effect between the input function and region ($F=2.69$, $p=0.048$). Subsequently, parametric maps of BP_{ND}^{super} and $BP_{ND}^{cerebellum}$ were compared pixel-by-pixel in each individual to identify subjects in whom the two input functions differed.

A similar pattern in the Bland-Altman plots was found in 10 out of 23 glioma patients (44 %), in both the tumour regions and tumour-free regions of the brain (Fig. 5), indicating good agreement between the BP_{ND} parametric maps derived from the two input functions. GLM analysis in this subgroup showed neither an effect of input function ($F=$

2.05 , $p=0.186$) nor a cross effect between the input function and region.

In 13 of 23 patients (56 %), the Bland-Altman plots and local regression analyses revealed consistently smaller, but correlated, BP_{ND}^{super} than $BP_{ND}^{cerebellum}$ values, again both inside and outside the tumours in the brain (Fig. 6). This finding is in keeping with the observation that TACs of the supervised cluster of GM remained slightly higher than those of the cerebellar GM throughout the acquisition (Fig. 6c), thus producing smaller BP_{ND} estimates. GLM analysis in this subgroup confirmed a significant effect of input function on BP_{ND} ($F=96.46$, $p<0.0001$) and a cross effect between the input function and region ($F=4.88$, $p=0.036$), indicating that BP_{ND}^{super} differed from $BP_{ND}^{cerebellum}$ across all ROIs in 56 % of our glioma patients.

The locations of significant binding were independent of the input function used. They remained identical in the two BP_{ND} maps of the same patient or control subject.

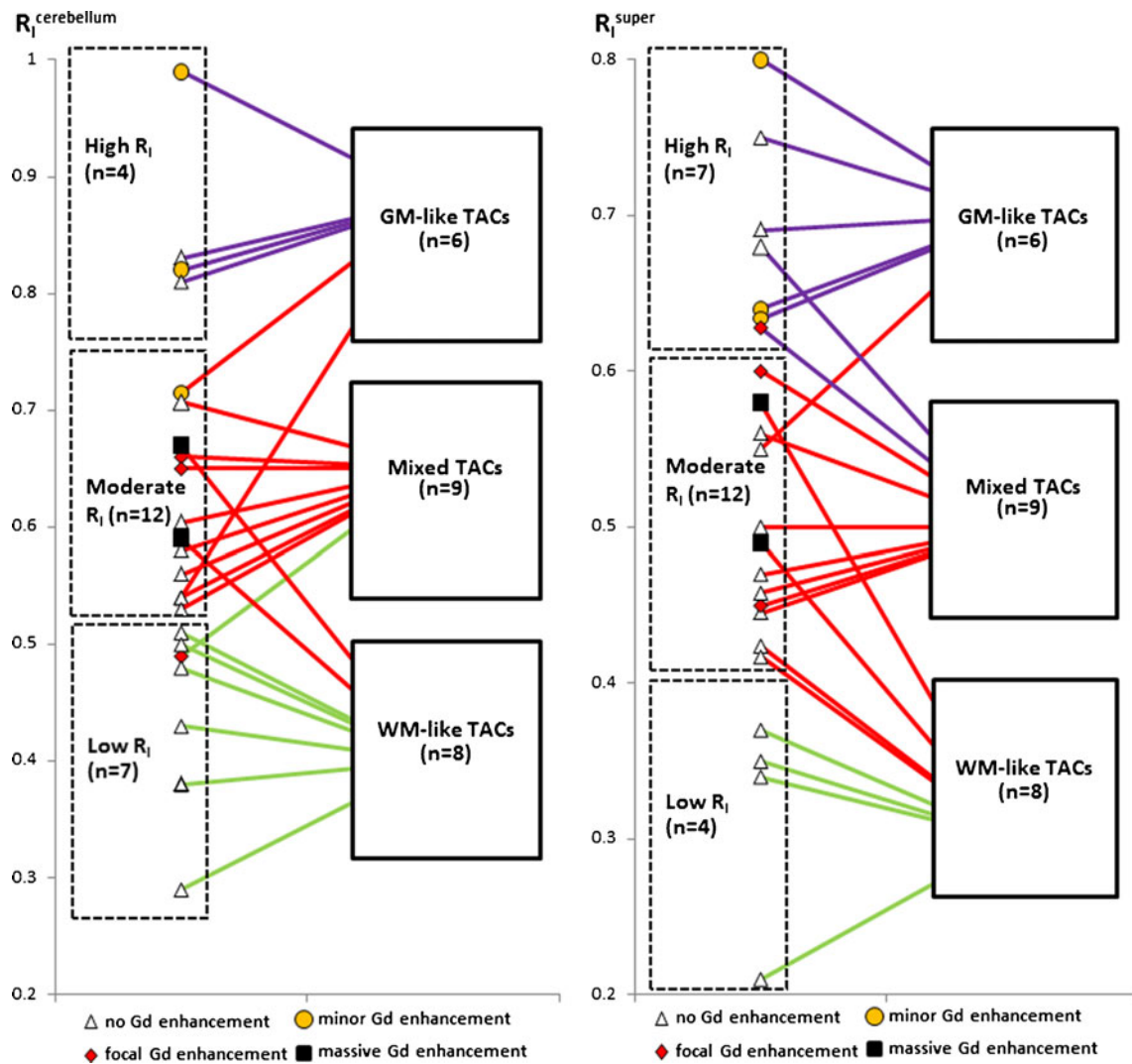


Fig. 3 Relationship among the three categories of tumour R_1 (calculated with cerebellar input or supervised cluster input) and the three types of tumour TACs

Neuropathology

The number of TSPO-positive neoplastic cells increased with tumour grade (Fig. 7) and the number was higher in GBMs. The results of the semiquantitative analysis are summarized in Tables 1 and 2. In addition, high-grade lesions demonstrated more intense immunolabelling (Fig. 7c). The number of microglia increased with tumour grade, but only a minority of them appeared to express TSPO. The majority of normal, preexisting vessels in low-grade astrocytomas and low-grade oligodendrogliomas showed TSPO-positive endothelial cells, although some degree of variability was observed between different regions of the same tumour and between different subjects. Interestingly, newly formed vessels and proliferative endothelium in GBMs conversely showed consistently low to negative TSPO.

Discussion

Understanding the different tumour TACs

One major finding of this study is the three types of tracer kinetics in gliomas, and the different kinetics between low-grade astrocytomas (WM-like TAC) and low-grade oligodendrogliomas (GM-like and mixed TACs). This difference is of clinical interest because the distinction between these two glioma subtypes is important but currently difficult on conventional neuroimaging. Such early distinction is valuable in therapeutic stratification and outcome prediction since oligodendrogliomas show better responses to chemotherapy and significantly improved overall survival than astrocytomas of a comparable grade [49].

There are several possible reasons for the different kinetics between low-grade astrocytomas and low-grade

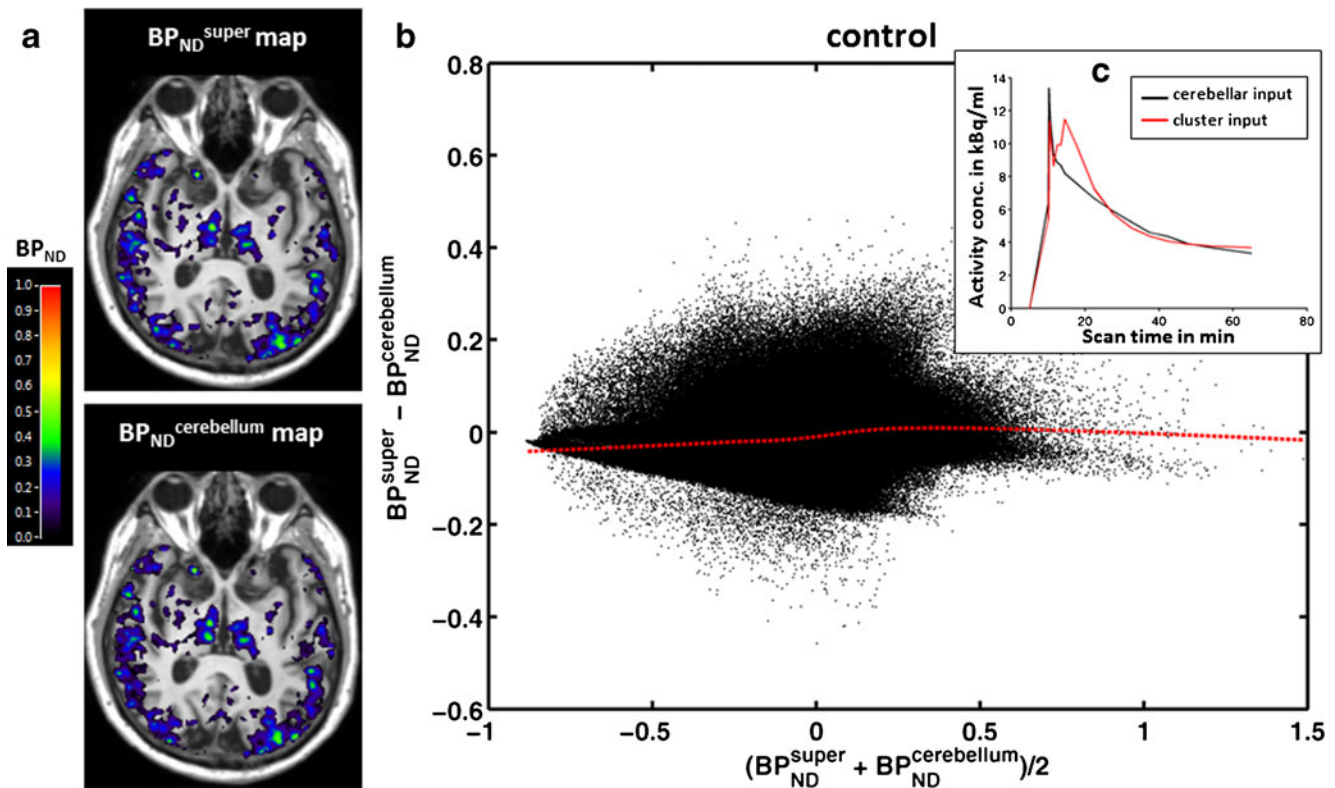


Fig. 4 Parametric maps of BP_{ND}^{super} and $BP_{ND}^{cerebellum}$ in a representative control subject (65-year-old man). **a** Parametric maps of BP_{ND}^{super} and $BP_{ND}^{cerebellum}$ superimposed on T1-weighted MR images; the colour bar indicates BP_{ND} values. **b** Pixel-by-pixel Bland-

Altman plot comparing the values from the two parametric maps. Each *black dot* is derived from a pixel in the brain and the *red dashed line* denotes local regression. **c** Corresponding individual TACs of the supervised cluster of GM (*red*) and cerebellar GM (*black*)

oligodendrogliomas. TSPO is known to form homopolymers, predominantly dimers and trimers, that seem to increase during cell proliferation and to complex with other mitochondrial proteins present in the outer and inner mitochondrial membrane as part of the mitochondrial permeability transition pore. In addition, the TSPO functions seem to be affected by tissue-specific and cell-specific proteins as well as the lipid compositions of the mitochondrial membranes [50]. Formation of different homopolymers or heteropolymers or differences in protein and lipid composition may be responsible for the different kinetics between astrocytomas and oligodendrogliomas. Although our histology results did not show obvious difference in endothelial TSPO between the two histotypes, increased vascularity in oligodendrogliomas [51] may also explain the kinetic behaviour similar to that in the GM in these tumours. Our results showed predominantly TSPO expression in neoplastic cells in both histotypes of glioma, which is in keeping with the findings of previous pathological studies on astrocytic tumours [27, 28], and suggests that microglia/macrophages do not interfere with $[^{11}C]$ -(R)PK11195 uptake in gliomas. Hence, the difference in kinetics between low-grade astrocytomas and oligodendrogliomas is less likely to be caused by different cellular sources of TSPO expression. A recent PET study on two anaplastic astrocytomas also indicated that

glioma-infiltrating microglia fail to express TSPO [31]. Nevertheless, further work is needed to investigate TSPO in oligodendrogliomas and the contribution of reactive astrocytes, endothelia and microglia to $[^{11}C]$ -(R)PK11195 binding.

In one low-grade astrocytoma with exceptional GM-like kinetics (patient 8), the tumour grade might have been underestimated. This 63-year-old patient underwent biopsy rather than surgical debulking, and the limited amount of tissue obtained might not have been representative of the grade. The patient showed clinical and radiological progression 6 months after the biopsy, a behaviour that is more in keeping with a HGG.

Eight HGGs with varying degrees of Gd enhancement (three slightly enhanced, three focally enhanced and two massively enhanced) were characterized by GM-like, mixed and WM-like kinetics, respectively (Table 2). This observation suggests a direct relationship between BBB status and tracer kinetic behaviour in these tumours. In the three patients with a mildly disturbed or relatively intact BBB, $[^{11}C]$ -(R)PK11195 accumulated in both the normal brain and tumour tissue rapidly, followed by a slightly slower washout from tumour tissue than from the GM. We believe that this subtle retention reflects binding in the tumours. In the two patients with a significantly damaged BBB, the tracer also accumulated in the tumours

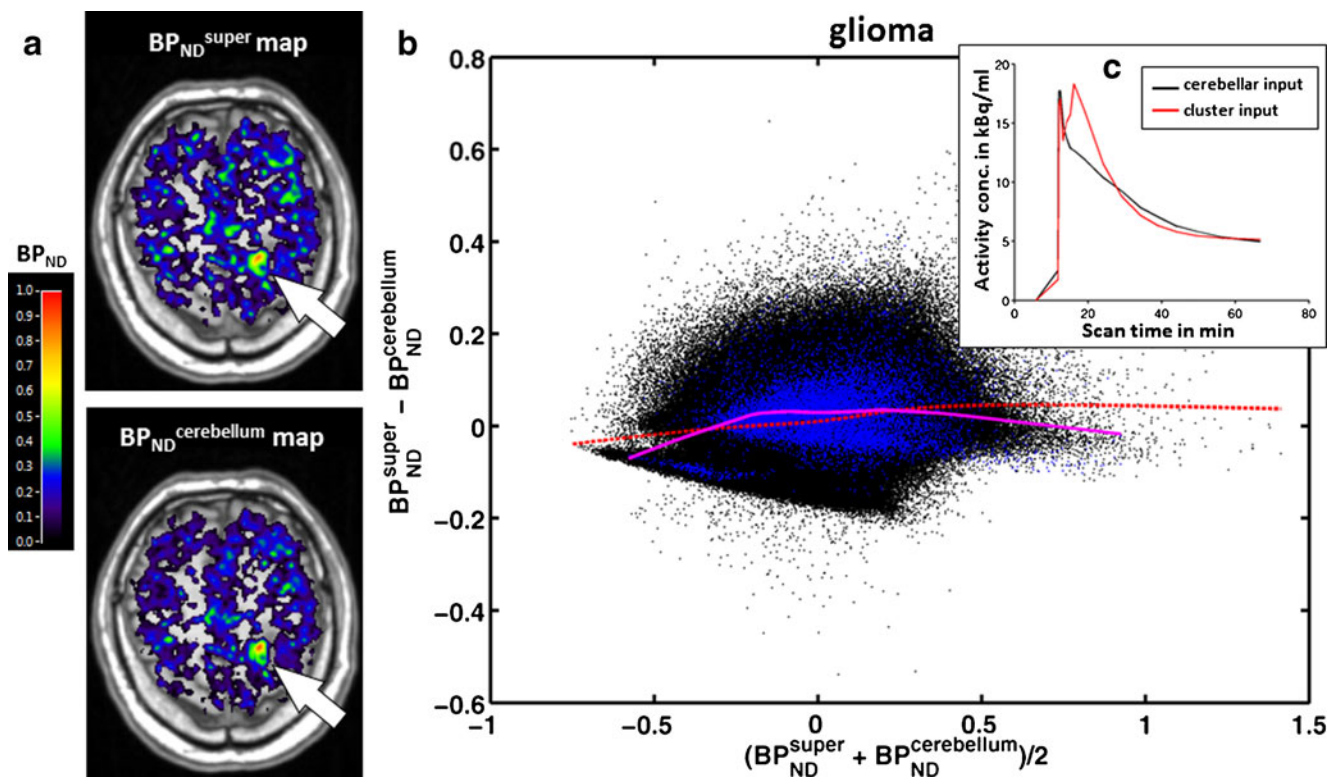


Fig. 5 Parametric maps of BP_{ND}^{super} and $BP_{ND}^{cerebellum}$ in a representative glioma patient (patient 10). **a** Parametric maps of BP_{ND}^{super} and $BP_{ND}^{cerebellum}$ superimposed on T1-weighted MR images. Note the high BP_{ND} area within the tumour (arrows $BP_{ND}^{super}=0.52\pm 0.14$, $BP_{ND}^{cerebellum}=0.52\pm 0.14$); the colour bar indicates BP_{ND} values. **b** Pixel-by-pixel Bland-Altman plot comparing the values from the two

parametric maps. Each *black dot* is derived from a pixel in the brain, and each *blue dot* from a pixel in the tumour; the *red dashed line* and *purple solid line* denote local regression in the brain pixels and tumour pixels, respectively. **c** Corresponding individual TACs of the supervised cluster of GM (*red*) and cerebellar GM (*black*)

quickly, but the washout from tumour tissue was much slower and stayed at a level higher than that in GM from 15 min after injection (Fig. 2). This retention reflected considerable $[^{11}C]$ -(R)PK11195 binding to the TSPO highly expressed by neoplastic cells and possibly macrophages infiltrated from the bloodstream. In the three patients with focal Gd enhancement indicating regional disruption of the BBB, the tracer behaved in a mixed fashion in-between GM-like and WM-like kinetics. It can be argued that different degrees of WM-like kinetics may be a characteristic of BBB leakage and subsequent $[^{11}C]$ -(R)PK11195 accumulation and elevated binding in these eight HGGs. However, since all three types of tumour TAC were detected in the nonenhancing gliomas, the impact of BBB leakage in determining the profiles of tracer uptake kinetics is limited. Other mechanisms such as tracer delivery and tumour heterogeneity may be more relevant.

$[^{11}C]$ -(R)PK11195 is highly lipophilic and it can cross the intact BBB by passive diffusion. Its delivery is not predominantly determined by BBB leakage. This is supported by our tumour R_1 data (both $R_1^{cerebellum}$ and R_1^{super} ; Fig. 3) where tumours with massive or focal Gd enhancement demonstrated only moderate R_1 . Therefore, the influence of tumour R_1 on tracer kinetics was investigated. The three categories of

tumour R_1 , especially the high and low categories, generally matched the three types of tumour uptake kinetics. This, together with the TAC grouping effect on R_1 , suggests that tracer delivery contributes in part to their kinetic behaviour within the tumours. Such an interpretation can be derived from either the $R_1^{cerebellum}$ or the R_1^{super} data, although the distribution of patients in the R_1 categories varied depending on the reference region used, which was caused by the different ranges of $R_1^{cerebellum}$ and R_1^{super} values. In addition, kinetic analysis revealed that the initial accumulation of $[^{11}C]$ -(R)PK11195 peaked at least to the level of the WM in all tumour TACs, indicating sufficient delivery of the radiotracer into the tumours. Subsequent binding was not hampered by the relatively low tumour R_1 in some patients in whom blood flow and/or tracer extraction in tumour regions may be less than that in the reference GM. Moreover, the inhomogeneous tracer kinetics across these tumours mirrors the heterogeneous nature of gliomas, and also reflects the fact that tumour uptake kinetic behaviour is mostly in the range between normal GM and WM. Overall, $[^{11}C]$ -(R)PK11195 proved to be a suitable radiotracer for glioma investigation, because it can be delivered sufficiently into the tumour, was not dependent on BBB leakage, and was taken up by the

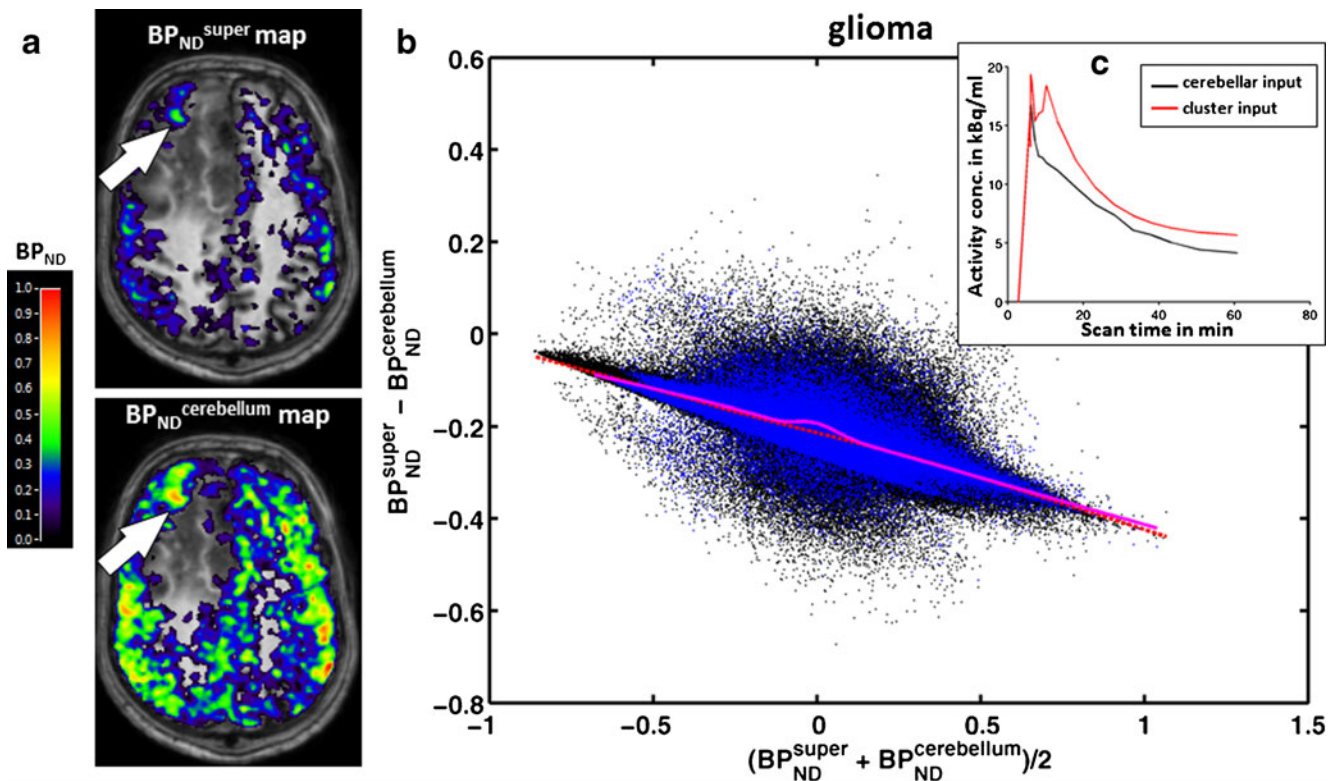


Fig. 6 Parametric maps of BP_{ND}^{super} and $BP_{ND}^{cerebellum}$ in a representative glioma patient (patient 4, the patient showing the maximal differences). **a** Parametric maps of BP_{ND}^{super} and $BP_{ND}^{cerebellum}$ superimposed on T1-weighted MR images. Note the high BP_{ND} area within the tumour (arrows $BP_{ND}^{super}=0.25\pm 0.09$, $BP_{ND}^{cerebellum}=0.52\pm 0.11$); the colour bar indicates BP_{ND} values. **b** Pixel-by-pixel Bland-

Altman plot comparing values from the two parametric maps. Each *black dot* is derived from a pixel in the brain, and each *blue dot* from a pixel in the tumour; the *red dashed line* and *purple solid line* denote local regression in the brain pixels and tumour pixels, respectively. **c** Corresponding individual TACs of the supervised cluster of GM (*red*) and cerebellar GM (*black*)

tumour within the framework of known kinetics. Finally, given the inhomogeneous uptake behaviour amongst gliomas, we stress that visual inspection of tumour TACs from dynamic

scanning is as informative as quantification of tumour/GM and tumour/WM ratios in kinetic analysis, especially with regard to atypical cases.

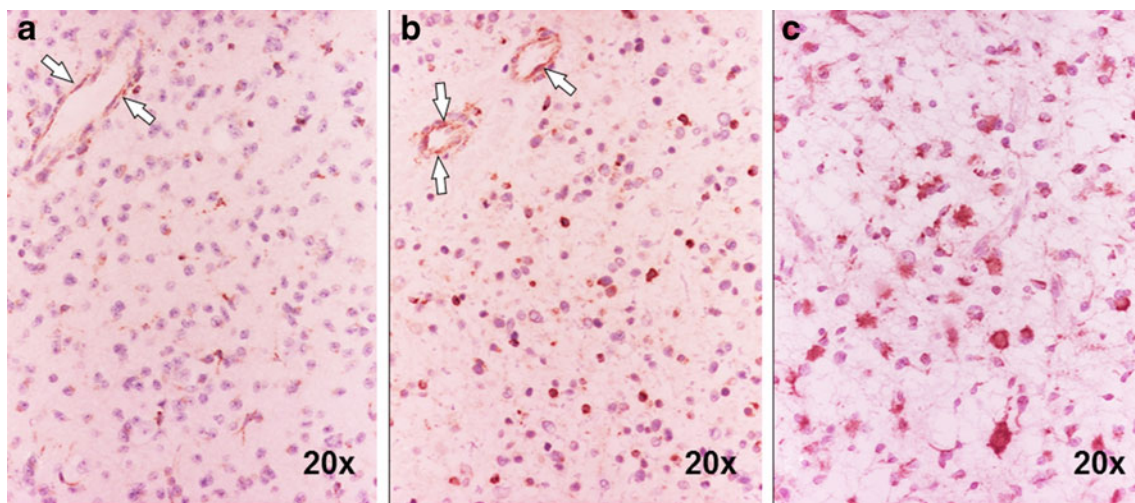


Fig. 7 TSPO expression in relation to tumour grade. **a** Patient 20 with low-grade oligodendroglioma, quantified as +: expression is limited to a few neoplastic cells; endothelial cells are positive (arrows). **b** Patient 17 with low-grade astrocytoma, quantified as ++: a higher number of

cells are TSPO-positive; endothelial cells are also positive (arrows). **c** Patient 19 with anaplastic astrocytoma, quantified as +++: an even higher number of cells are TSPO-positive. Immunoperoxidase, $\times 20$

Performance of different reference tissue input functions

Previous [^{11}C]-(*R*)PK11195 PET studies in various neurological disorders and healthy ageing subjects employed SRTM with either cerebellum or cluster analysis as the input function [2, 10, 20–22, 52, 53]. Consequently, we also adopted these previously used methods and assessed their performance in our glioma and control cohorts. For the cerebellar input function, bilateral and not unilateral cerebellar GM was used in gliomas for consistency with controls, and also because of its larger volume and thus reduced noise.

Supervised clustering versus cerebellum input

Pixel-by-pixel comparisons of BP_{ND} parametric maps generated with supervised cluster analysis or cerebellar GM as a reference tissue allowed us to compare the properties of these two input functions in the absence of a plasma input function. In control subjects, Bland-Altman plots and local regression, together with comparisons of regional values, demonstrated no systematic difference between the two approaches. Similar findings were seen in 10 of 23 glioma patients. Such good agreement indicates that these two reference input functions led to consistent results in all the control subjects and approximately half of glioma patients.

However, in the other 13 of 23 patients, BP_{ND} values in both the tumour and brain using the supervised cluster input function were consistently smaller than those calculated using the cerebellar input function. This observation indicates either underestimation of BP_{ND} by the supervised cluster input and/or overestimation by the cerebellar input, suggesting that at least one of the approaches may be subject to bias. Underestimation of BP_{ND} using the supervised cluster analysis might be caused by (1) pixels in the tumour being mistakenly included in the reference cluster, or (2) brain tissue outside the tumour in patients differing from that in controls. An internal mask derived from the PET data is used for clustering in the supervised cluster approach with six classes [4], and although low uptake areas in the tumour will be masked out, high uptake foci might still be included in the reference cluster. Hence, the first problem is indeed likely to occur in gliomas with high [^{11}C]-(*R*)PK11195 binding, especially those demonstrating GM-like kinetics that are sufficiently similar to the kinetics in the GM. In fact, focal or diffuse high [^{11}C]-(*R*)PK11195 uptake was observed in seven out of these 13 tumours, three of which also showed GM-like kinetics. The inclusion of those tumour pixels with high [^{11}C]-(*R*)PK11195 signals in the reference cluster will lead to underestimation of BP_{ND} . Regarding the second problem, nonneoplastic cerebral regions might be affected by intrahemispheric and transhemispheric diaschisis [54, 55], oedema or abnormal electroactivity induced by seizures, any of which could trigger local or diffuse neuroinflammatory responses and thus increased [^{11}C]-(*R*)PK11195 uptake by

activated microglia [56–58]. It is possible that the supervised clustering could be biased by such background changes and extract abnormal pixels as reference. Indeed, visual inspection of the GM class probability maps revealed that certain pixels around the tumour margin or even within the tumour were identified in some cases. Hence, a modified supervised cluster analysis [26], with further supervision by masking out the tumour pixels prior to clustering, would be likely to improve the robustness of reference region extraction. To further study all the aforementioned phenomena, absolute quantification with plasma input function would be required.

On the other hand, overestimation of BP_{ND} using cerebellar GM as an input function could occur due to ‘contamination’ by small volumes of cerebellar WM because of imperfect segmentation or the partial volume effect. Although such contamination altered the performance of cerebellar GM input when compared with supervised cluster input, it should not affect the use of cerebellar GM as a reference tissue, since previous studies have adopted the total cerebellum as the input function [2, 10, 20–22]. In the less common situation in which a glioma localizes in the cerebellum (mainly paediatric cases; beyond the scope of this study), the use of the unaffected cerebellar hemisphere as the reference tissue might still be preferred. Supervised cluster analysis extracts a cluster of GM pixels from the whole brain including the cerebellum [4]. Therefore, it could possibly sample pixels with GM-like kinetics (if any) from a tumour located there. On balance, we preferred the use of cerebellar GM input function because it provided a conservative measure of [^{11}C]-(*R*)PK11195 binding and the uptake differences between subject groups. This implies that when a difference in binding is detected it is more likely to represent a true positive result than differences demonstrated by the supervised cluster approach.

Nevertheless, without the plasma input, we cannot give a definitive answer as to which input function performed better, nor can we guarantee that the cerebellar GM is absolutely spared and does not contain increased specific binding (to activated microglia) when compared with controls. Moreover, SRTM suffers from bias in discrepancies in a blood volume fraction between target and reference regions. This effect is further increased by the presence of TSPO in blood vessel walls [19]. Taking into account the blood volume fraction, the vascular corrected SRTM results in higher BP_{ND} estimates than the SRTM [19]. Therefore, it may represent a better model for glioma investigation, especially those with increased blood volume. This hypothesis will be investigated in our future work.

In addition, our imaging data showed that, despite certain systematic differences in the BP_{ND} estimates in some subjects depending on the input function used, the overall anatomical pattern of significant [^{11}C]-(*R*)PK11195 binding did not alter in the same subject.

In conclusion, the three types of tracer kinetics in gliomas are determined in part by the tracer delivery. They also

reflect the heterogeneous nature of gliomas, and confirm that [^{11}C](R)PK11195 is a suitable radiotracer for glioma imaging because of its unimpeded delivery to tumour tissue and its well-characterized kinetics. Tracer kinetic analysis is a valuable tool in the study of TSPO expression in gliomas with potential for in vivo discrimination between low-grade astrocytomas and low-grade oligodendrogliomas. Supervised cluster input and cerebellar GM input produced BP_{ND} estimates in good agreement with one another in approximately half of the glioma patients, but showed consistent discrepancies, albeit correlated BP_{ND} , in the other half. However, the cerebellar input was preferred in our study based on theoretical and practical considerations.

Acknowledgments We thank the patients and healthy volunteers who participated in this study, and the staff involved in the scanning, especially Dr. Adam McMahon and Mr. Michael Green for radioligand synthesis, Mr. Jose Anton for image reconstruction and Dr. Christopher Kobylecki for scanning the volunteers, and the radiographers Ms. Eleanor Duncan-Rouse and Mr. Gerrit Helms Van Der Vegte. The research leading to these results received funding from the European Union's Seventh Framework Programme (FP7/2007-2013) under grant agreement no. HEALTH-F2-2011-278850 (INMiND), the Manchester Integrating Medicine and Innovative Technology programme (Science Bridges Project R108094), and the Astro Fund. Prof. Federico Turkheimer was supported by the MRC programme grant 'Quantitative methodologies for Positron Emission Tomography' (G1100809/1). Ms. Konstantina Karabatsou, Mr. Ajit Sofat, Mr. James Leggate, Dr. Ioannis Trigonis, Dr. David Coope, Dr. Gerard Thompson, Dr. Calvin Soh, Mr. Andrew Brodbelt, Dr. Kumar Das and Dr. Daniel Crooks provided clinical support and/or helped with patient identification.

Conflicts of interest None.

Open Access This article is distributed under the terms of the Creative Commons Attribution License which permits any use, distribution, and reproduction in any medium, provided the original author(s) and the source are credited.

References

- Kassiou M, Meikle SR, Banati RB. Ligands for peripheral benzodiazepine binding sites in glial cells. *Brain Res Brain Res Rev.* 2005;48:207–10.
- Schuitmaker A, van Berckel BN, Kropholler MA, Veltman DJ, Scheltens P, Jonker C, et al. SPM analysis of parametric (R)-[^{11}C]PK11195 binding images: plasma input versus reference tissue parametric methods. *Neuroimage.* 2007;35:1473–9.
- Banati RB. Visualising microglial activation in vivo. *Glia.* 2002;40:206–17.
- Turkheimer FE, Edison P, Pavese N, Roncaroli F, Anderson AN, Hammers A, et al. Reference and target region modeling of [^{11}C](R)-PK11195 brain studies. *J Nucl Med.* 2007;48:158–67.
- Cosenza-Nashat M, Zhao ML, Suh HS, Morgan J, Natividad R, Morgello S, et al. Expression of the translocator protein of 18 kDa by microglia, macrophages and astrocytes based on immunohistochemical localization in abnormal human brain. *Neuropathol Appl Neurobiol.* 2008;35:306–28.
- Shah F, Hume SP, Pike VW, Ashworth S, McDermott J. Synthesis of the enantiomers of [N-methyl- ^{11}C]PK 11195 and comparison of their behaviours as radioligands for PK binding sites in rats. *Nucl Med Biol.* 1994;21:573–81.
- Banati RB, Newcombe J, Gunn RN, Cagnin A, Turkheimer F, Heppner F, et al. The peripheral benzodiazepine binding site in the brain in multiple sclerosis: quantitative in vivo imaging of microglia as a measure of disease activity. *Brain.* 2000;123(Pt 11):2321–37.
- Cagnin A, Brooks DJ, Kennedy AM, Gunn RN, Myers R, Turkheimer FE, et al. In-vivo measurement of activated microglia in dementia. *Lancet.* 2001;358:461–7.
- Gerhard A, Banati RB, Goerres GB, Cagnin A, Myers R, Gunn RN, et al. [^{11}C](R)-PK11195 PET imaging of microglial activation in multiple system atrophy. *Neurology.* 2003;61:686–9.
- Gerhard A, Schwarz J, Myers R, Wise R, Banati RB. Evolution of microglial activation in patients after ischemic stroke: a [^{11}C](R)-PK11195 PET study. *Neuroimage.* 2005;24:591–5.
- Tai YF, Pavese N, Gerhard A, Tabrizi SJ, Barker RA, Brooks DJ, et al. Imaging microglial activation in Huntington's disease. *Brain Res Bull.* 2007;72:148–51.
- Venneti S, Lopresti BJ, Wiley CA. The peripheral benzodiazepine receptor (Translocator protein 18kDa) in microglia: from pathology to imaging. *Prog Neurobiol.* 2006;80:308–22.
- Gerhard A, Pavese N, Hotton G, Turkheimer F, Es M, Hammers A, et al. In vivo imaging of microglial activation with [^{11}C](R)-PK11195 PET in idiopathic Parkinson's disease. *Neurobiol Dis.* 2006;21:404–12.
- Kropholler MA, Boellaard R, Schuitmaker A, van Berckel BN, Luurtsema G, Windhorst AD, et al. Development of a tracer kinetic plasma input model for (R)-[^{11}C]PK11195 brain studies. *J Cereb Blood Flow Metab.* 2005;25:842–51.
- Kropholler MA, Boellaard R, Schuitmaker A, Folkersma H, van Berckel BN, Lammertsma AA. Evaluation of reference tissue models for the analysis of [^{11}C](R)-PK11195 studies. *J Cereb Blood Flow Metab.* 2006;26:1431–41.
- Lammertsma AA, Hume SP. Simplified reference tissue model for PET receptor studies. *Neuroimage.* 1996;4:153–8.
- Schuitmaker A, van Berckel BN, Kropholler MA, Kloet RW, Jonker C, Scheltens P, et al. Evaluation of methods for generating parametric (R)-[^{11}C]PK11195 binding images. *J Cereb Blood Flow Metab.* 2007;27:1603–15.
- Gunn RN, Lammertsma AA, Hume SP, Cunningham VJ. Parametric imaging of ligand-receptor binding in PET using a simplified reference region model. *Neuroimage.* 1997;6:279–87.
- Tomasi G, Edison P, Bertoldo A, Roncaroli F, Singh P, Gerhard A, et al. Novel reference region model reveals increased microglial and reduced vascular binding of ^{11}C (R)-PK11195 in patients with Alzheimer's disease. *J Nucl Med.* 2008;49:1249–56.
- Kropholler MA, Boellaard R, van Berckel BN, Schuitmaker A, Kloet RW, Lubberink MJ, et al. Evaluation of reference regions for (R)-[^{11}C]PK11195 studies in Alzheimer's disease and mild cognitive impairment. *J Cereb Blood Flow Metab.* 2007;27:1965–74.
- Banati RB, Goerres GW, Myers R, Gunn RN, Turkheimer FE, Kreutzberg GW, et al. [^{11}C](R)-PK11195 positron emission tomography imaging of activated microglia in vivo in Rasmussen's encephalitis. *Neurology.* 1999;53:2199–203.
- Cagnin A, Myers R, Gunn RN, Lawrence AD, Stevens T, Kreutzberg GW, et al. In vivo visualization of activated glia by [^{11}C](R)-PK11195-PET following herpes encephalitis reveals projected neuronal damage beyond the primary focal lesion. *Brain.* 2001;124:2014–27.
- Doble A, Malgouris C, Daniel M, Daniel N, Imbault F, Basbaum A, et al. Labelling of peripheral-type benzodiazepine binding sites in human brain with [^3H]PK 11195: anatomical and subcellular distribution. *Brain Res Bull.* 1987;18:49–61.
- Ashburner J, Haslam J, Taylor G, Cunningham VJ, Jones T. A cluster analysis approach for the characterization of dynamic PET data. In: Myers R, Cunningham V, Bailey D, Jones T, editors.

- Quantitative functional brain imaging with positron emission tomography. San Diego: Academic; 1996. p. 301–6.
25. Myers R, Gunn RN, Cunningham VJ, Banati RB, Jones T. Cluster analysis and the reference tissue model in the analysis of clinical [^{11}C]PK11195 PET. *J Cereb Blood Flow Metab.* 1999;19:S789.
 26. Yaqub M, van Berckel BN, Schuitemaker A, Hinz R, Turkheimer FE, Tomasi G, et al. Optimization of supervised cluster analysis for extracting reference tissue input curves in (R)-[^{11}C]PK11195 brain PET studies. *J Cereb Blood Flow Metab.* 2012;32:1600–8.
 27. Miettinen H, Kononen J, Haapasalo H, Helen P, Sallinen P, Harjuntausta T, et al. Expression of peripheral-type benzodiazepine receptor and diazepam binding inhibitor in human astrocytomas: relationship to cell proliferation. *Cancer Res.* 1995;55:2691–5.
 28. Vlodayvsky E, Soustiel JF. Immunohistochemical expression of peripheral benzodiazepine receptors in human astrocytomas and its correlation with grade of malignancy, proliferation, apoptosis and survival. *J Neurooncol.* 2007;81:1–7.
 29. Junck L, Olson JM, Ciliax BJ, Koeppe RA, Watkins GL, Jewett DM, et al. PET imaging of human gliomas with ligands for the peripheral benzodiazepine binding site. *Ann Neurol.* 1989;26:752–8.
 30. Pappata S, Cornu P, Samson Y, Prenant C, Benavides J, Scatton B, et al. PET study of carbon-11-PK 11195 binding to peripheral type benzodiazepine sites in glioblastoma: a case report. *J Nucl Med.* 1991;32:1608–10.
 31. Takaya S, Hashikawa K, Turkheimer FE, Mottram N, Deprez M, Ishizu K, et al. The lack of expression of the peripheral benzodiazepine receptor characterises microglial response in anaplastic astrocytomas. *J Neurooncol.* 2007;85:95–103.
 32. Badie B, Schartner JM, Paul J, Bartley BA, Vorpahl J, Preston JK. Dexamethasone-induced abolition of the inflammatory response in an experimental glioma model: a flow cytometry study. *J Neurosurg.* 2000;93:634–9.
 33. Kaur C, Dheen ST, Ling EA. From blood to brain: amoeboid microglial cell, a nascent macrophage and its functions in developing brain. *Acta Pharmacol Sin.* 2007;28:1087–96.
 34. Drew PD, Chavis JA. Inhibition of microglial cell activation by cortisol. *Brain Res Bull.* 2000;52:391–6.
 35. Cremer JE, Hume SP, Cullen BM, Myers R, Manjil LG, Turton DR, et al. The distribution of radioactivity in brains of rats given [N-methyl- ^{11}C]PK 11195 in vivo after induction of a cortical ischaemic lesion. *Int J Rad Appl Instrum B.* 1992;19:159–66.
 36. Hong IK, Chung ST, Kim HK, Kim YB, Son YD, Cho ZH. Ultra fast symmetry and SIMD-based projection-backprojection (SSP) algorithm for 3-D PET image reconstruction. *IEEE Trans Med Imaging.* 2007;26:789–803.
 37. Hinz R, Jones M, Bloomfield PM, Boellaard R, Turkheimer FE, Tyrrell PJ. Reference tissue kinetics extraction from [^{11}C]- (R)-PK11195 scans on the High Resolution Research Tomograph (HRRT). *Neuroimage.* 2008;41:T65.
 38. Cizek J, Herholz K, Vollmar S, Schrader R, Klein J, Heiss WD. Fast and robust registration of PET and MR images of human brain. *Neuroimage.* 2004;22:434–42.
 39. Ashburner J, Friston KJ. Unified segmentation. *Neuroimage.* 2005;26:839–51.
 40. Hammers A, Chen CH, Lemieux L, Allom R, Vossos S, Free SL, et al. Statistical neuroanatomy of the human inferior frontal gyrus and probabilistic atlas in a standard stereotaxic space. *Hum Brain Mapp.* 2007;28:34–48.
 41. Hammers A, Allom R, Koeppe MJ, Free SL, Myers R, Lemieux L, et al. Three-dimensional maximum probability atlas of the human brain, with particular reference to the temporal lobe. *Hum Brain Mapp.* 2003;19:224–47.
 42. Innis RB, Cunningham VJ, Delforge J, Fujita M, Gjedde A, Gunn RN, et al. Consensus nomenclature for in vivo imaging of reversibly binding radioligands. *J Cereb Blood Flow Metab.* 2007;27:1533–9.
 43. Anderson AN, Pavese N, Edison P, Tai YF, Hammers A, Gerhard A, et al. A systematic comparison of kinetic modelling methods generating parametric maps for [^{11}C]- (R)-PK11195. *Neuroimage.* 2007;36:28–37.
 44. Wyss MT, Hofer S, Hefti M, Bartschi E, Uhlmann C, Treyer V, et al. Spatial heterogeneity of low-grade gliomas at the capillary level: a PET study on tumor blood flow and amino acid uptake. *J Nucl Med.* 2007;48:1047–52.
 45. Tang BN, Sadeghi N, Branle F, De Witte O, Wikler D, Goldman S. Semi-quantification of methionine uptake and flair signal for the evaluation of chemotherapy in low-grade oligodendroglioma. *J Neurooncol.* 2005;71:161–8.
 46. Imai Y, Kohsaka S. Intracellular signaling in M-CSF-induced microglia activation: role of Iba1. *Glia.* 2002;40:164–74.
 47. Bland JM, Altman DG. Measuring agreement in method comparison studies. *Stat Methods Med Res.* 1999;8:135–60.
 48. Geisttanger A, Berding C, Vorberg E, Herlan M. Local regression: a new approach for measurement system comparison analysis. *Clin Chem Lab Med.* 2008;46:1211–9.
 49. Van den Bent MJ, Reni M, Gatta G, Vecht C. Oligodendroglioma. *Crit Rev Oncol Hematol.* 2008;66:262–72.
 50. Rupprecht R, Papadopoulos V, Rammes G, Baghai TC, Fan J, Akula N, et al. Translocator protein (18 kDa) (TSPO) as a therapeutic target for neurological and psychiatric disorders. *Nat Rev Drug Discov.* 2010;9:971–88.
 51. Cha S, Tihan T, Crawford F, Fischbein NJ, Chang S, Bollen A, et al. Differentiation of low-grade oligodendrogliomas from low-grade astrocytomas by using quantitative blood-volume measurements derived from dynamic susceptibility contrast-enhanced MR imaging. *AJNR Am J Neuroradiol.* 2005;26:266–73.
 52. Folkersma H, Boellaard R, Yaqub M, Kloet RW, Windhorst AD, Lammertsma AA, et al. Widespread and prolonged increase in (R)-[^{11}C]PK11195 binding after traumatic brain injury. *J Nucl Med.* 2011;52:1235–9.
 53. Schuitemaker A, van der Doef TF, Boellaard R, van der Flier WM, Yaqub M, Windhorst AD, et al. Microglial activation in healthy aging. *Neurobiol Aging.* 2012;33:1067–72.
 54. Feeney DM, Baron JC. Diaschisis. *Stroke.* 1986;17:817–30.
 55. Andrews RJ. Transhemispheric diaschisis. A review and comment. *Stroke.* 1991;22:943–9.
 56. Shinonaga M, Chang CC, Suzuki N, Sato M, Kuwabara T. Immunohistological evaluation of macrophage infiltrates in brain tumors. Correlation with peritumoral edema. *J Neurosurg.* 1988;68:259–65.
 57. Choi J, Nordli Jr DR, Alden TD, DiPatri Jr A, Laux L, Kelley K, et al. Cellular injury and neuroinflammation in children with chronic intractable epilepsy. *J Neuroinflammation.* 2009;6:38.
 58. Najjar S, Pearlman D, Miller DC, Devinsky O. Refractory epilepsy associated with microglial activation. *Neurologist.* 2011;17:249–54.